Materials Today Energy 22 (2021) 100885

Contents lists available at ScienceDirect

Materials Today Energy

journal homepage: www.journals.elsevier.com/materials-today-energy/

In-situ constructed destabilization reaction of $LiBH_4$ wrapped with graphene toward stable hydrogen storage reversibility

Jikai Ye, Guanglin Xia*, Xuebin Yu**

Department of Materials Science, Fudan University, Shanghai 200433, China

ARTICLE INFO

Article history:
Received 15 July 2021
Received in revised form
24 September 2021
Accepted 14 October 2021
Available online 25 October 2021

Keywords:
Hydrogen storage
Lithium borohydride
Reversibility
Destabilization reaction

ABSTRACT

Building destabilization reaction of $LiBH_4$ with high gravimetric and volumetric capacity has been regarded as one of the most effective ways to improve its hydrogen storage performance. These destabilization reactions, however, suffer from low efficiency and severe phase separation upon hydrogen storage, resulting in poor reversibility of $LiBH_4$. Herein, the construction of $LiBH_4$ destabilized by Al wrapped by graphene is realized by an *in-situ* solid–gas reaction of LiH and Al resulting from the dehydrogenation of $LiAlH_4$ and diborane. Owing to the uniform formation of LiH around Al nanoparticles on a molecular level, the homogeneous distribution of $LiBH_4$ around Al nanoparticles with intimate contact could be achieved, which, coupled with the significant decrease of their particle sizes down to the nanometer size, effectively promotes the destabilization reaction between $LiBH_4$ and Al. As a result, a single-step dehydrogenation reaction between $LiBH_4$ and Al towards the complete dehydrogenation of $LiBH_4$ with the formation of AlB_2 and AlLi is demonstrated at 400°C. More importantly, induced by the enhanced destabilization reaction efficiency between $LiBH_4$ and Al, the complete dehydrogenation and hydrogenation of $LiBH_4$ with a reversible capacity of 4.49 wt% after 5 cycles could be well preserved owing to the structural support role of graphene.

1. Introduction

The development of hydrogen energy is in urgent need induced by the increasing demand to build a clean and sustainable society [1–3]. The lack of an efficient and safe way to storage hydrogen with high gravimetric and volumetric capacity, however, poses a critical challenge for the large-scale application of hydrogen energy [4–8]. Among all the potential hydrogen storage techniques, solid-state hydrogen storage in metal hydrides attracts tremendous attention owing to its unique safety characteristics and high theoretical gravimetric and volumetric storage capacity [9–15]. In this respect, lithium borohydride ($LiBH_4$) is particularly favored owing to its extremely high gravimetric hydrogen capacity (18.5 wt%) and volumetric hydrogen density (121 kg H_2 m^{-3}) [16–19]. Nevertheless, induced by the strong ionic/covalent bonding between the constituent elements of $LiBH_4$, the standard reaction enthalpy for the decomposition of $LiBH_4$ reaches ~67 kJ mol^{-1} H_2, corresponding to a theoretical operating temperature of 410°C at 1 atm, which cannot satisfy the practical requirements for proton exchange membrane fuel cells [20–22]. Moreover, only half of the hydrogen content could be desorbed from $LiBH_4$ below 600°C owing to its high kinetic barrier, and, even under extremely harsh conditions of 600°C and 35 MPa hydrogen, only partial reversibility could be achieved, which remains a critical challenge for the practical application of $LiBH_4$ as hydrogen storage materials [23–25].

Theoretically, lowering the thermodynamic stability of $LiBH_4$ would be one of the most effective strategy to reduce its operating temperature for hydrogen storage [20,26–28]. For instance, the reaction enthalpy for the hydrogen storage of $LiBH_4$ could be reduced to only 40.5 kJ mol^{-1} H_2 because of the generation of AlB_2 through the thermodynamic destabilization reaction between $LiBH_4$ and Al [29]. As a result, the equilibrium temperature for the reversible hydrogen storage of $LiBH_4$ could be theoretically reduced to 188°C under 1 atm H_2, 220°C lower than that of pure $LiBH_4$. Detailed investigations on the reactions between $LiBH_4$ and Al from various sources with various $LiBH_4$-to-Al ratios [29–37] demonstrate the relatively stable reversibility of the $LiBH_4$/Al system through the formation of AlB_2 and AlLi as the dehydrogenation products. Unfortunately, owing to the high reactivity of $LiBH_4$ and

* Corresponding author.
** Corresponding author.
E-mail addresses: xiaguanglin@fudan.edu.cn (G. Xia), yuxuebin@fudan.edu.cn (X. Yu).

https://doi.org/10.1016/j.mtener.2021.100885
2468-6069/

Al, the traditional method to synthesize the $LiBH_4$–Al system is limited to mechanical milling with uncontrollable distribution and poor physical contact between $LiBH_4$ and Al. It leads to limited reaction capacity with only partial formation of AlB_2, which thus weakens the destabilizing effect on the dehydrogenation of $LiBH_4$ [33,35]. Furthermore, the insufficient contact between $LiBH_4$ and Al would also result in the partial decomposition of $LiBH_4$ alone with the formation of relatively stable $Li_2B_{12}H_{12}$, thus hindering the complete reversibility of the hydrogen storage system [38]. In addition, the sluggish transportation of elements, especially across the phases between $LiBH_4$ and Al, results in slow reaction kinetics, and hence the operating temperature of Al-destabilized $LiBH_4$ is still over 400°C. More importantly, the particle growth and agglomeration during the cycling hydrogenation and dehydrogenation process exacerbate the phase separation of $LiBH_4$ and Al, which further prevents the destabilization reaction between $LiBH_4$ and Al and hence leads to poor reversibility.

Herein, to promote the interaction between $LiBH_4$ and Al towards advanced hydrogen storage performance, we report *in-situ* construction of $LiBH_4$ on the surface of Al nanoparticles (NPs) wrapped by graphene ($LiBH_4$–Al@G) through a solid–gas reaction between diborane and LiH homogeneously distributed with Al NPs. As schematically illustrated in Fig. 1a, LiH and Al NPs with uniform distribution on a molecular level was first fabricated via the self-decomposition of $LiAlH_4$ supported on graphene using a solvent impregnation method. Subsequently, LiH NPs around Al NPs was transformed into $LiBH_4$ through the solid–gas reaction with diborane, which leads to the homogeneous formation of $LiBH_4$ around Al NPs with intimate contact and thus promotes the destabilization reaction between $LiBH_4$ and Al. In addition, the decrease of particle size of both $LiBH_4$ and Al down to the nanometer scale effectively reduces the transportation pathway of hydrogen and mass, leading to a single-step reaction between $LiBH_4$ and Al toward the complete dehydrogenation of $LiBH_4$ with the favorable formation of AlB_2 and AlLi at a temperature as low as 400°C, which is approximately 200°C lower than that of its bulk counterpart. More importantly, the phase separation between $LiBH_4$ and Al NPs could be remarkably alleviated owing to their uniform distribution on graphene layers acting as the structural support, and, as a result, complete dehydrogenation and hydrogenation could be effectively achieved for the $LiBH_4$–Al composite wrapped by graphene with a systematic hydrogen capacity of approximately 4.49 wt% within 5 cycles.

2. Results and discussions

$LiAlH_4$ homogeneously distributed onto graphene was first fabricated through a facile solvent impregnation method, and, hence, the loading ratio of $LiAlH_4$ could be easily adjusted by changing the mass ratio between $LiAlH_4$ and graphene. The as-synthesized samples are denoted as LAH@G-*x* with different loading ratios of $LiAlH_4$. After the solvent impregnation of $LiAlH_4$, X-ray diffraction (XRD) patterns (Fig. S1a) verify the characteristic peaks belonging to $LiAlH_4$, indicating the presence of $LiAlH_4$.

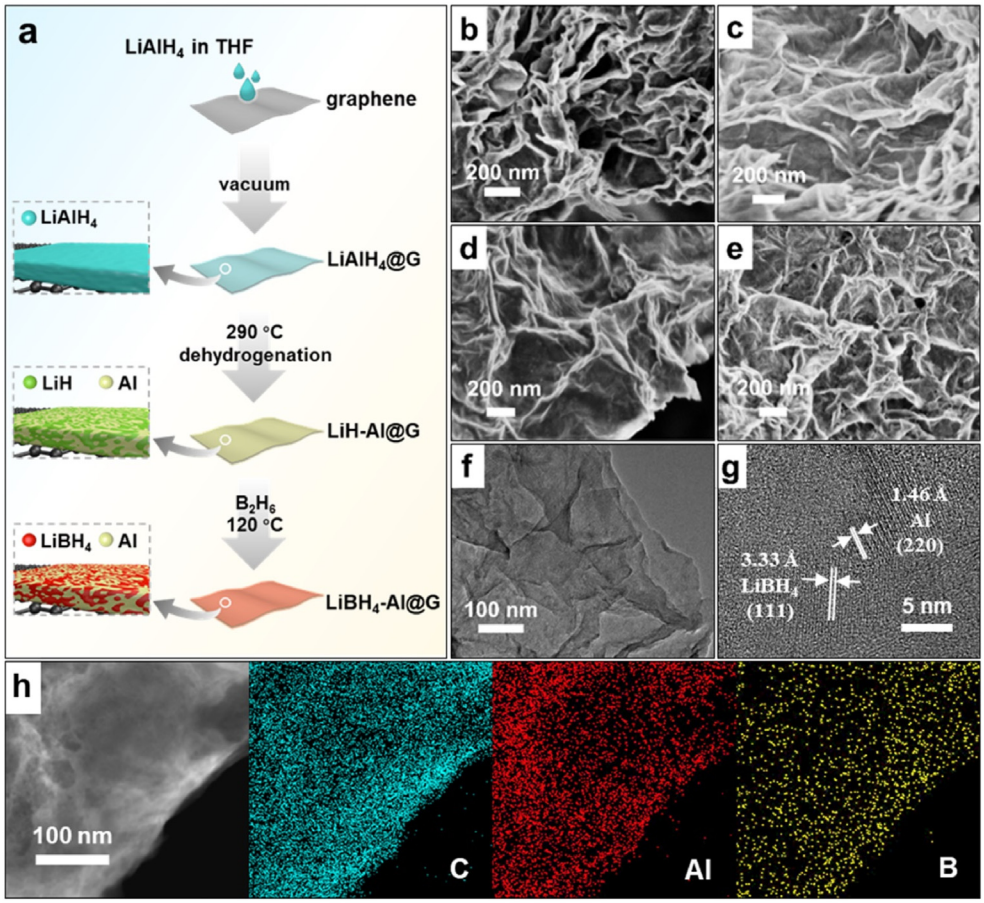

Fig. 1. a) Schematic illustration of the synthesis of $LiBH_4$–Al@G composite. SEM images of b) LAH@G-1, c) LAH@G-2, d) LBH-Al@G-1, e) LBH-Al@G-2. f) TEM, g) HRTEM, and h) STEM and the corresponding elemental mapping images of LBH-Al@G-2. HRTEM, high-resolution TEM; SEM, scanning electron microscope; STEM, scanning TEM; TEM, transmission electron microscope.

Moreover, Fourier-transform infrared (FT-IR) spectra of LAH@G-2 (Fig. S2), which exhibit vibrational peaks at 1782 cm^{-1} and 1643 cm^{-1}, corresponding to the stretching mode of $LiAlH_4$, and 883 cm^{-1} and 838 cm^{-1}, corresponding to the bending mode of $LiAlH_4$, provide additional evidence to the existence of $LiAlH_4$. Scanning electron microscope (SEM) images reveal the homogeneous distribution of $LiAlH_4$ on graphene at a relatively lower loading ratio (LAH@G-1, LAH@G-2) without observation of obvious agglomeration (Fig. 1b and c), which could be further confirmed by the transmission electron microscope (TEM) image and scanning TEM (STEM) images with elemental mapping results (Fig. S3). The high-resolution TEM (HRTEM) image presents typical lattice fringes of ~2.49 Å and ~2.43 Å, which could be indexed to the (142(—)) and (241(—)) planes of $LiAlH_4$, respectively, suggesting the successful formation of $LiAlH_4$ on graphene. The elemental mapping results verify that the Al of $LiAlH_4$ and C of graphene are homogeneously distributed through the whole composite, indicating the uniform distribution of $LiAlH_4$ on graphene, which provides stable structural support for uniform formation of $LiBH_4$ around Al with good dispersion. As expected, clear agglomeration of $LiAlH_4$ could be observed upon the increase of the loading ratio (Fig. S4). Upon heating, $LiAlH_4$ supported on graphene could be transformed into LiH and Al with intimate physical contact at a molecular level, accompanied with the release of hydrogen [39]. Temperature-programmed desorption (TPD) curves of all $LiAlH_4$@G samples exhibit a two-step desorption (Fig. S5), which corresponds well with the expected decomposition of $LiAlH_4$ with the formation of LiH and Al as evidenced by the XRD patterns (Fig. S1b) and FT-IR spectra (Fig. S2).

Subsequently, by virtue of the reaction between LiH and B_2H_6 (*i.e.* $2LiH + B_2H_6 \rightarrow 2LiBH_4$) [40,41], LiH NPs surrounded by Al NPs in the dehydrogenated $LiAH_4$@G was *in-situ* transformed into $LiBH_4$, and, hence, $LiBH_4$ and Al with intimate contact wrapped by graphene, denoted as LBH-Al@G-*y*, could be uniformly synthesized. The correspondence between LAH@G-*x* and LBH-Al@G-*y* composites with their loading ratio is illustrated in detail in the experimental section (Table S1). Scanning electron microscope (Fig. 1d and e) and TEM (Fig. 1f) images and the corresponding elemental mapping results (Fig. 1h) demonstrate that the as-synthesized LBH-Al@G-1 and LBH-Al@G-2 inherit the structure of LAH@G-1 and LAH@G-2, in which $LiBH_4$ and Al are distributed homogeneously distributed on the surface of graphene. No conspicuous particles, however, could be observed on graphene, suggesting the layer-by-layer formation of ultra-small size of as-formed Al and $LiBH_4$ particles on the surface of graphene. Fortunately, the HRTEM image (Fig. 1g) confirms the co-existence of lattice fringes of ~3.33 Å, corresponding to (111) planes of Al, and ~1.46 Å, corresponding to (220) planes of $LiBH_4$, indicating the formation of $LiBH_4$ and Al with intimate contact. Although only visible peaks of Al could be identified in the XRD results (Fig. 2a), the successful formation of $LiBH_4$ could be clearly evidenced by the presence of its characteristic B—H bonds in the FT-IR spectra (Fig. 2b).

The dehydrogenation performance of the as-synthesized $LiBH_4$—Al@G samples was subsequently investigated using the TPD method. As shown in Fig. 2c and d, the ball-milled composite of $LiBH_4$ and Al with a molar ratio of 1:1 (denoted as BM $LiBH_4$—Al) exhibits an onset dehydrogenation temperature of 400°C and two major dehydrogenation peaks at 461°C and 543°C could be attributed to the decomposition of $LiBH_4$ with the formation of AlB_2 and LiH and the subsequent decomposition of LiH towards the formation of AlLi, respectively, as verified by XRD results (Fig. S6). Continuous dehydrogenation at temperatures over 575°C, however, could also be observed for BM $LiBH_4$—Al owing to the inhomogeneous contact between $LiBH_4$ and Al. Upon heating to 600°C, 6.8 wt% of hydrogen, corresponding to only 83% of its theoretical hydrogen content, could be released from BM $LiBH_4$—Al, which provides additional evidence to the insufficient reaction between $LiBH_4$ and Al due to their inhomogeneous distribution with large particle sizes (Fig. S7). It should be noted that the hydrogen capacity in this work is calculated based on the mass of the whole system. With the addition of graphene, the peak temperature for the dehydrogenation of $LiBH_4$ is lowered to 413°C for BM LBH-Al/G-2 and 450°C for BM LBH-Al/G-4, respectively, indicating the catalytic role of graphene in promoting the hydrogen desorption performance of $LiBH_4$, which coincides well with the previously reported results [41—44]. By comparison, although all $LiBH_4$—Al@G samples exhibit comparable onset dehydrogenation temperature at ~300°C, the peak temperature for the dehydrogenation of $LiBH_4$ is decreased significantly compared with the ball-milled counterparts. Particularly, a peak temperature of 405°C was observed for the dehydrogenation of LBH-Al@G-4, which is about 45°C lower than BM LBH-Al/G-4. More interestingly, in terms of LBH-Al@G-1 and LBH-Al@G-2, the two-step dehydrogenation process for the combination of $LiBH_4$ and Al merges into one single hydrogen desorption peak at 381 and 391°C, respectively, the latter of which is 22°C lower than that of its ball-milled counterpart. After dehydrogenation at 400°C, XRD results (Fig. 2e) of LBH-Al@G-2 demonstrate the formation of AlLi and the high-resolution B 1s and Al 2p XPS spectra (Fig. S8) exhibits the characteristic peaks of AlB_2 and AlLi alloys [45,46], accompanied with the complete absence of B—H bonds in the relative FT-IR spectra (Fig. 2f). The absence of characteristic peaks of the newly formed AlB_2 in the XRD results should be attributed to its low content and/or its amorphous nature. These results provide direct evidence to the complete dehydrogenation of $LiBH_4$ after the single-step decomposition of LBH-Al@G-2 at a temperature as low as 400°C, which could be attributed to the synergistic effect of nano-size effect and the catalytic role of graphene in promoting the chemical reaction between $LiBH_4$ and Al. Mass spectrum (MS) results confirm that only H_2 could be released from LBH-Al@G-2 upon heating to 600°C (Fig. S9). By comparison, only characteristic peaks of Al or LiH could be observed in the XRD patterns of BM LBH-Al/G-2 without observable formation of AlLi and the characteristic peaks of B—H bonds could be clearly detected in the FT-IR spectra, indicating the inefficient reaction between Al and $LiBH_4$ with the incomplete dehydrogenation of $LiBH_4$. It directly demonstrates that the reduction of particle size could not only significantly reduce the dehydrogenation temperature of the $LiBH_4$—Al system, but also promote the destabilization reaction between $LiBH_4$ and Al towards complete dehydrogenation. Unfortunately, upon increasing the loading ratio of $LiBH_4$ and Al, extra dehydrogenation peaks at temperatures above 500°C could be observed for LBH-Al@G-3 and LBH-Al@G-4, comparable to their ball-milled counterparts, indicating the incomplete reaction between $LiBH_4$ and Al due to the partial agglomeration of $LiBH_4$ and Al particles on the surface of graphene (Fig. S10).

Isothermal dehydrogenation kinetics of the graphene-wrapped $LiBH_4$—Al composites were investigated at various temperatures (Fig. 2g). Upon heating at the temperature of 340°C, 2.56 wt% of hydrogen could be released from LBH-Al@G-1 within 66 min, corresponding to 70% of its theoretical capacity. Although the dehydrogenation capacity could be increased to 3.49 wt% for LBH-Al@G-3, the dehydrogenation content is reduced to 62% of its theoretical capacity because of the partial agglomeration of $LiBH_4$ and Al particles on the surface of graphene induced by the increased loading ratio (Fig. S10). By comparison, the hydrogen desorption capacity of LBH-Al@G-2 could reach 3.83 wt% under identical condition, corresponding to 78% of its theoretical capacity, which is much higher than that of its ball-milled counterpart and other graphene-wrapped $LiBH_4$—Al composites. Moreover, a capacity as high as

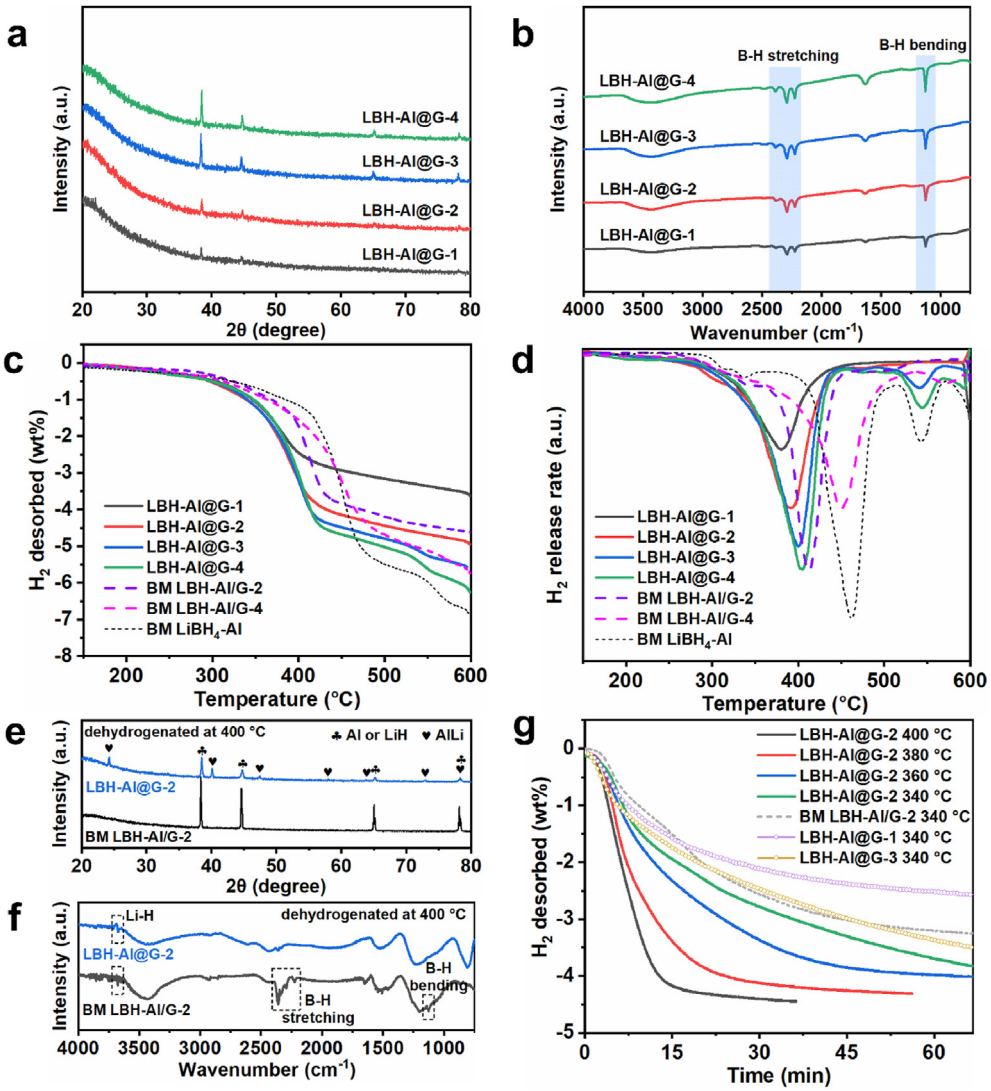

Fig. 2. a) XRD patterns, b) FT-IR spectra of $LiBH_4$—Al@G samples. c) TPD and d) its derivative curves of LBH-Al@G-1, LBH-Al@G-2, LBH-Al@G-3 and LBH-Al@G-4, including BM LBH-Al/G-2, BM LBH-Al/G-4 and BM $LiBH_4$—Al for comparison. e) XRD patterns and f) FT-IR spectra of the products of LBH-Al@G-2 and BM LBH-Al/G-2 after dehydrogenation at 400°C. g) Isothermal dehydrogenation curves of LBH-Al@G-2 at 340, 360, 380 and 400°C, including LBH-Al@G-1, LBH-Al@G-3 and BM LBH-Al/G-2 at 340°C for comparison. The as-obtained hydrogen desorption capacity has an error within ±1%. FT-IR, Fourier-transform infrared; XRD, X-ray diffraction.

4.49 wt% is released from LBH-Al@G-2 upon increasing the temperature to 400°C within the period of only 36 min. To gain better understanding of the improvement in the hydrogen desorption kinetics of LBH-Al@G-2, its apparent activation energies (E_a) were quantitatively calculated based on the Arrhenius equation through fitting the experimental dehydriding kinetics at various temperatures (Fig. S11). The E_a value for the dehydrogenation from LBH-Al@G-2 was determined to be 56.37 ± 6.93 kJ mol^{-1}, which, as shown in Fig. S12, is much lower than that for its ball-milled counterpart (i.e. 75.23 ± 1.00 kJ mol^{-1}). This result confirms the significant enhancement of hydrogen storage performance of $LiBH_4$—Al systems due to the significant reduction of particle size of both $LiBH_4$ and Al down to the nanometer scale, which could effectively improve the destabilization reaction between Al and $LiBH_4$ with intimate contact.

The cycling performance of graphene-wrapped $LiBH_4$—Al composites, which is the key aspect and also a major bottleneck for the practical application of $LiBH_4$ as hydrogen storage materials, was further investigated at 400°C through the volumetric method. As shown in Fig. 3a and b, only a reversible capacity of 3.08 wt%, corresponding to a capacity retention of 76.1%, could be obtained for BM LBH-Al/G-2 after only 3 cycles due to the significant phase separation between $LiBH_4$ and Al as evidenced by the SEM image (Fig. S13). No obvious formation of $LiBH_4$ could be detected by the XRD results, and only weak characteristic peaks of B—H bonds could be observed in the FT-IR spectra (Figs. S14 and S15), which provides further evidence to the poor reversibility of ball-milled $LiBH_4$—Al composites. In strong contrast, a reversible hydrogen capacity as high as 4.49 wt% could be observed for LBH-Al@G-2 under identical conditions, and, more importantly, the stable reversibility could be completely preserved for the *in-situ*—formed $LiBH_4$—Al supported on graphene even after 5 cycles. The absence of B—H bonds in the FT-IR spectra (Fig. 3c) of LBH-Al@G-2 after 5 cycles of hydrogen desorption process demonstrates the complete dehydrogenation of $LiBH_4$, corresponding well with the cycling capacity tests. Although no characteristic diffraction peaks of $LiBH_4$ could be detected by XRD results (Fig. 3d) of LBH-Al@G-2 after 5 cycles of hydrogen absorption process due to the amorphous nature of the thus-regenerated $LiBH_4$, the obvious formation of B—H bonds could be validated by the relative FT-IR spectra (Fig. 3c). In addition,

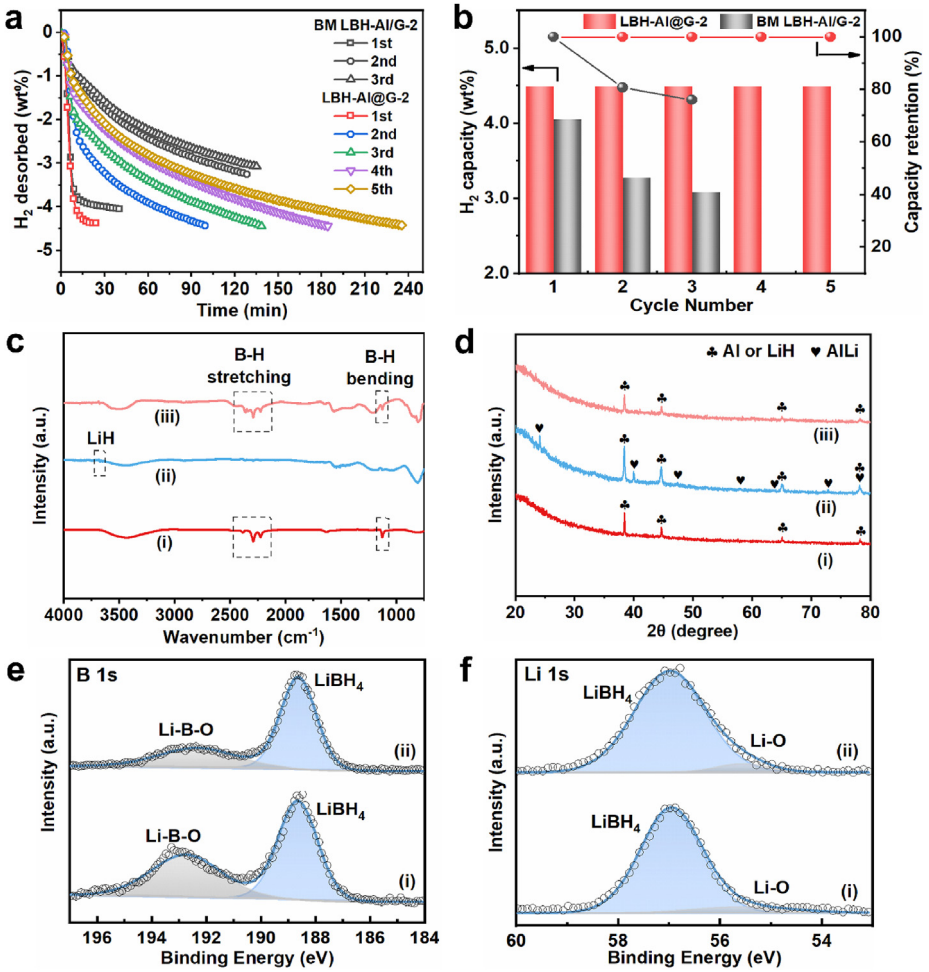

Fig. 3. a) Reversible dehydrogenation curves of LBH-Al@G-2 in comparison with BM LBH-Al/G-2 at 400°C, and the corresponding b) cyclic dehydrogenation capacities with its reversible ratio normalized to the dehydrogenation capacity exhibited in the first cycle. The as-obtained hydrogen desorption capacity has an error within ±1%. Note that all hydrogenation procedure is performed under 10 MPa H_2 at 400°C for 10 h. c) FT-IR spectra and d) XRD patterns of LBH-Al@G-2 after (i) 1st and (iii) 5th cycle of hydrogenation and (ii) 5th cycle of dehydrogenation. High-resolution e) B 1s and f) Li 1s XPS spectra of (i) LBH-Al@G-2 and (ii) its product after 5th cycle of hydrogenation. FT-IR, Fourier-transform infrared; XPS, X-ray photoelectron spectroscopy; XRD, X-ray diffraction.

only the characteristic peaks of $LiBH_4$ could be observed in the high-resolution B 1s and Li 1s XPS spectra of LBH-Al@G-2 after 5 cycles of hydrogen absorption process (Fig. 3e and f) [47–49], which provides further evidence to the stable reversibility of $LiBH_4$. Hence, the operating reaction of LBH-Al@G-2 at 400°C could be concluded as $2LiBH_4 + 2Al \leftrightarrow AlB_2 + AlLi + LiH + 7/2H_2$. The promoted formation of AlB_2 and AlLi induced by the significant decrease of particle size could thermodynamically improve the reversibility of $LiBH_4$, which could be further demonstrated by the enhanced reversibility of ball-milled $LiBH_4$–Al composite in comparison with bulk $LiBH_4$. Induced by the formation of AlB_2 and AlLi from ball-milled $LiBH_4$–Al composite upon heating to 600°C as verified by XRD results (Fig. S6), 82.5% of hydrogen could be reversibly desorbed relative to that of the first cycle after rehydrogenation under 10 MPa H_2 at 400°C (Fig. S16). By comparison, the ball-milled $LiBH_4$ could only desorb 52.6% of hydrogen relative to its first cycle of dehydrogenation under identical condition.

The morphology changes in the graphene-wrapped $LiBH_4$–Al composites were subsequently investigated at the end of 5 cycles of hydrogenation process (Fig. 4a). Severe phase separation between Al and $LiBH_4$ could be clearly observed for ball-milled composite of $LiBH_4$–Al and graphene upon proceeding the reversible hydrogen storage performance, which coincides well with the obvious capacity degradation observed in the long-term cycling tests (Fig. S17). By comparison, the uniform distribution of $LiBH_4$ and Al on graphene could be well preserved during the cycling hydrogenation and dehydrogenation process for LBH-Al@G-2 due to the structural support role of graphene (Fig. 4b and c). A slight increase of sizes of $LiBH_4$ and Al particles, however, could be observed induced by both the melting of $LiBH_4$ and the reversible nucleation of $LiBH_4$ and Al, which is comparable to the phenomenon observed for LBH-Al@G-1 (Fig. S18). The average particle size of the $LiBH_4$–Al composites is increased to 27.8 nm after 5 cycles of hydrogenation process from 23.6 nm after 3 cycles of hydrogenation process (Figs. S19 and S20), which would lead to the degradation of the dehydrogenation kinetics as observed in Fig. 3a. To gain better understanding on the reversible performance of LBH-Al@G-2, 5 additional cycles of hydrogen storage process were performed (Fig. S21). It could be clearly observed that, upon the further proceeding of cycling performance, the degradation of the dehydrogenation kinetics of LBH-Al@G-2 is alleviated, which correlates well with the limited increase of the average particle size of the $LiBH_4$–Al composite (i.e. 32.3 nm after 10 cycles of hydrogenation process as shown in Fig. S22). As a result, the degradation of dehydrogenation kinetics could be reasonably attributed to the slight increase of particle size of the $LiBH_4$–Al composite upon

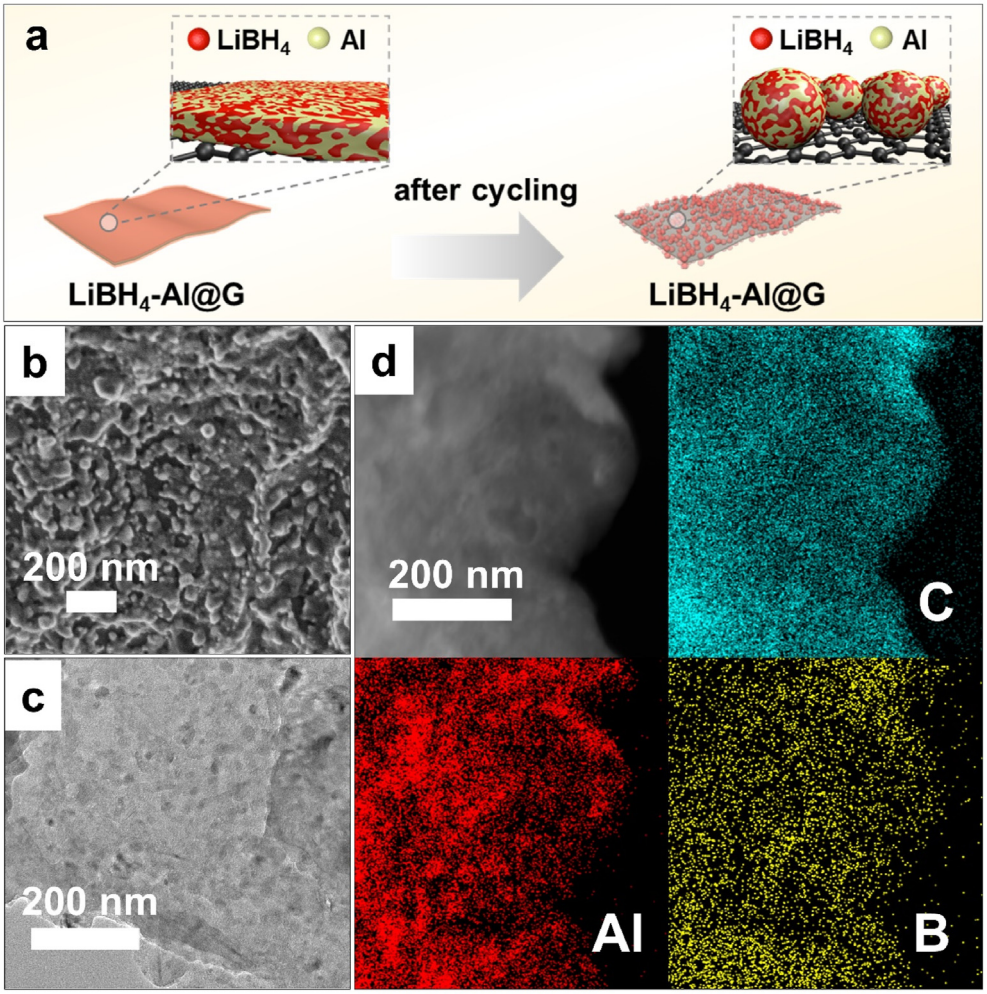

Fig. 4. a) Schematic illustration of the change at the surface of $LiBH_4$—Al@G after cycles of dehydrogenation and hydrogenation. b) SEM, c) TEM and d) STEM and corresponding elemental mapping images of the products of LBH-Al@G-2 after 5th cycle of hydrogenation. SEM, scanning electron microscope; STEM, scanning TEM; TEM, transmission electron microscope.

cycling, which would increase the diffusion pathway of hydrogen and mass transportation pathway and hence lead to the slight degradation of the dehydrogenation kinetics. Fortunately, induced by the space-confinement effect of graphene, the particle growth is significantly limited with an average particle size of 32.3 nm even after 10 cycles of hydrogenation process and the homogeneous distribution of $LiBH_4$—Al composite on graphene is well maintained (Fig. 4d), contributing to the complete reversibility of $LiBH_4$ upon cycling, which hence is much superior than the graphene-confined $LiBH_4$ NPs as reported in literatures [44,50].

3. Conclusions

In conclusion, we have developed an effective strategy to improve the cyclability for hydrogen storage of $LiBH_4$ by building graphene-wrapped destabilization reaction between $LiBH_4$ and Al via an *in-situ* solid—gas reaction. Taking advantage of graphene-supported $LiAlH_4$ NPs as the precursor, which results in the formation of LiH and Al with a molar ratio of 1:1 upon facile dehydrogenation process, the destabilization reaction of $LiBH_4$ by Al NPs with intimate contact on a molecular level could be effectively constructed based on the subsequent reaction between LiH and diborane. Induced by the significant decrease of particle size of both $LiBH_4$ and Al down to the nanometer scale with intimate contact, a complete dehydrogenation with a capacity of 4.49 wt% could be achieved within only 36 min. More importantly, the reversible hydrogen storage capacity of 4.49 wt% could be well preserved after 5 cycles of hydrogenation and dehydrogenation process due to the space-confinement role of graphene. We believe this concept might open up new sights in constructing stable destabilization reaction toward efficient and effective hydrogen storage performance.

4. Experimental section

All samples were operated in an argon-filled glovebox with O_2 and $H_2O < 0.1$ ppm.

4.1. Synthesis of $LiAlH_4$@G

Typically, certain amount of $LiAlH_4$ (2 M in THF) and graphene with different ratios was dispersed in THF under ultrasonication for 1 h in a Schlenk tube which was sealed with tapes under Ar protection. Then, a Schlenk line was used to remove THF under dynamic vacuum at 80°C overnight. The obtained black powder with different $LiAlH_4$ loading ratios was denoted as LAH@G-*x* ($x = 1, 2, 3, 4$).

4.2. Synthesis of $LiBH_4$—Al@G

The synthesis of $LiBH_4$—Al@G was achieved through a solid—gas reaction method as we previously reported [41]. Specifically, the as-prepared $LiAlH_4$@G decomposed through a temperature-programmed-desorption process from room temperature to 290°C with a heating rate of 5°C min^{-1}. The product was then heated under a mixed atmosphere of B_2H_6/H_2 at 120°C for 24 h B_2H_6 was provided by the decomposition (>90°C) of a superfluous ball-milled mixture of $LiBH_4$ and $ZnCl_2$ with a molar ratio of 1:2. This process was performed in a high-pressure autoclave which was first sealed in the Ar-filled glovebox and was then replaced with 1 MPa H_2. The as-obtained $LiBH_4$—Al@G were denoted as LBH-Al@G-*y* ($y = 1, 2, 3, 4$). The correspondence between LAH@G-*x* and LBH-Al@G-*y* composites with their loading ratio is summarized in Table S1.

4.3. Synthesis of ball-milled $LiBH_4$—Al/G

Typically, $LiBH_4$, Al and graphene with the same ratio in LBH-Al@G-2 and LBH-Al@G-4 composites were sealed in a jar with tapes under Ar atmosphere protection and ball-milled for 2 h with a ball-to-powder weight ratio of 40:1 using a planetary QM-1SP2. The milling speed was controlled to be 400 rpm by alternating between 30 min of milling and 15 min of rest. The as-milled samples are denoted as BM LBH-Al/G-2 and BM LBH-Al/G-4, respectively.

4.4. Synthesis of ball-milled $LiBH_4$—Al

The preparation of ball-milled $LiBH_4$—Al is the same as that of BM LBH-Al/G composites except for the absence of graphene. The $LiBH_4$ to Al molar ratio is 1. The as-milled sample is denoted as BM $LiBH_4$—Al.

4.5. Material characterizations

The phase composition of powdery samples was characterized by X-ray diffraction (XRD, D8 advance, Bruker AXS) with Cu Kα (λ = 1.5418 Å), and all samples were covered with an amorphous tape (with a broad peak at $2\theta \approx 20^\circ$) to avoid possible reactions between samples and air during measurement. The morphology of samples was characterized using a field-emission scanning electron microscope (FE-SEM, JEOL 7500FA, Tokyo, Japan) and a transmission electron microscope (TEM, JEOL 2011 F, Tokyo, Japan). To avoid oxidation of $LiBH_4$, all the samples for TEM measurement were first dispersed on Cu grids in the glovebox and then rapidly transferred into the chambers for testing within a few seconds. X-ray photoelectron spectroscopy (XPS) results were obtained on a PerkinElmer PHI 5000C ESCA system equipped with a dual X-ray source, adopting a Mg Kα (1253.6 eV) anode with a hemispherical energy analyzer. The air-sensitive $LiBH_4$-contained composites were transferred with a specially designed vessel in the glovebox to avoid any contamination from air. The background pressure during data acquisition was maintained below 10^{-6} Pa, and all the measurements were conducted at a pass energy of 93.90 eV. All binding energies were calibrated by contaminant carbon (C 1s = 284.8 eV). Fourier-transform infrared (FT-IR, Magna-IR 550 II, Nicolet) analysis was adopted to verify the chemical bonding. All the powder samples were grinded with KBr and compressed into a translucent thin chip for FT-IR characterization.

4.6. Hydrogen storage measurements

Temperature-programmed desorption (TPD), isothermal dehydrogenation tests, and corresponding hydrogenation process of the as-prepared samples were conducted on a home-built high-pressure gas sorption apparatus (HPSA), which was carefully calibrated by adopting $LaNi_5$ as a reference sample in terms of hydrogen storage capacity and guaranteed an accuracy of ±1%. The hydrogen capacity (wt%) of all samples was calculated based on the total mass of the whole system, including the mass of the used graphene. Approximately 30 mg of as-prepared sample was used for each test. Temperature-programmed desorption tests were performed at a heating rate of 5°C min^{-1}. Both TPD and isothermal dehydrogenation process were conducted under an initial pressure <0.001 MPa. Cycle performance was tested isothermally at 400°C. The hydrogenation process was realized under an initial hydrogen pressure of 10 MPa at 400°C for 10 h. The composition of gases released was detected by a mass spectrometer (MS; Hiden QIC 20) with a heating rate of 5°C min^{-1}.

Credit author statement

Jikai Ye: Investigation, Data curation, Formal analysis, Writing - original draft. **Guanglin Xia:** Conceptualization, Methodology, Supervision, Writing – review & editing. **Xuebin Yu:** Supervision, Writing – review & editing.

Declaration of competing interest

The authors declare that they have no known competing financial interests or personal relationships that could have appeared to influence the work reported in this paper.

Acknowledgements

This work was partially supported by the National Key R&D Program of China (No. 2020YFA0406204), National Science Fund for Distinguished Young Scholars (51625102), the National Natural Science Foundation of China (51971065, 51901045, U2130208), the Science and Technology Commission of Shanghai Municipality (No. 21ZR1407500), the Innovation Program of Shanghai Municipal Education Commission (2019-01-07-00-07-E00028), and the Programs for Professor of Special Appointment (Eastern Scholar) at Shanghai Institutions of Higher Learning.

Appendix A. Supplementary data

Supplementary data to this article can be found online at https://doi.org/10.1016/j.mtener.2021.100885.

References

[1] L. Schlapbach, A. Züttel, Hydrogen-storage materials for mobile applications, Nature 414 (2001) 353–358.
[2] X.B. Yu, Z.W. Tang, D.L. Sun, L.Z. Ouyang, M. Zhu, Recent advances and remaining challenges of nanostructured materials for hydrogen storage applications, Prog. Mater. Sci. 88 (2017) 1–48.
[3] V.A. Yartys, M.V. Lototskyy, E. Akiba, R. Albert, V.E. Antonov, J.R. Ares, M. Baricco, N. Bourgeois, C.E. Buckley, J.M. Bellosta von Colbe, J.C. Crivello, F. Cuevas, R.V. Denys, M. Dornheim, M. Felderhoff, D.M. Grant, B.C. Hauback, T.D. Humphries, I. Jacob, T.R. Jensen, P.E. de Jongh, J.M. Joubert, M.A. Kuzovnikov, M. Latroche, M. Paskevicius, L. Pasquini, L. Popilevsky, V.M. Skripnyuk, E. Rabkin, M.V. Sofianos, A. Stuart, G. Walker, H. Wang, C.J. Webb, M. Zhu, Magnesium based materials for hydrogen based energy storage: past, present and future, Int. J. Hydrogen Energy 44 (2019) 7809–7859.

[4] R. Mohtadi, S.-i. Orimo, The renaissance of hydrides as energy materials, Nat. Rev. Mater. 2 (2016) 16091.
[5] H.Y. Zhang, G.L. Xia, J. Zhang, D.L. Sun, Z.P. Guo, X.B. Yu, Graphene-tailored thermodynamics and kinetics to fabricate metal borohydride nanoparticles with high purity and enhanced reversibility, Adv. Energy Mater. 8 (2018) 1702975.
[6] K. Chen, L. Ouyang, H. Zhong, J. Liu, H. Wang, H. Shao, Y. Zhang, M. Zhu, Converting H^+ from coordinated water into H^- enables super facile synthesis of $LiBH_4$, Green Chem. 21 (2019) 4380–4387.
[7] S. Wang, M. Gao, K. Xian, Z. Li, Y. Shen, Z. Yao, Y. Liu, H. Pan, $LiBH_4$ nanoconfined in porous hollow carbon nanospheres with high loading, low dehydrogenation temperature, superior kinetics, and favorable reversibility, ACS Appl. Energy Mater. 3 (2020) 3928–3938.
[8] W. Chen, L. You, G.L. Xia, X.B. Yu, A balance between catalysis and nanoconfinement towards enhanced hydrogen storage performance of $NaAlH_4$, J. Mater. Sci. Technol. 79 (2021) 205–211.
[9] S.-i. Orimo, Y. Nakamori, J.R. Eliseo, A. Züttel, C.M. Jensen, Complex hydrides for hydrogen storage, Chem. Rev. 107 (2007) 4111–4132.
[10] Y. Jia, C. Sun, S. Shen, J. Zou, S.S. Mao, X. Yao, Combination of nanosizing and interfacial effect: future perspective for designing Mg-based nanomaterials for hydrogen storage, Renew. Sustain. Energy Rev. 44 (2015) 289–303.
[11] Q. Lai, M. Paskevicius, D.A. Sheppard, C.E. Buckley, A.W. Thornton, M.R. Hill, Q. Gu, J. Mao, Z. Huang, H.K. Liu, Z. Guo, A. Banerjee, S. Chakraborty, R. Ahuja, K.-F. Aguey-Zinsou, Hydrogen storage materials for mobile and stationary applications: current state of the art, ChemSusChem 8 (2015) 2789–2825.
[12] G.L. Xia, L.J. Zhang, X.W. Chen, Y.Q. Huang, D.L. Sun, F. Fang, Z.P. Guo, X.B. Yu, Carbon hollow nanobubbles on porous carbon nanofibers: an ideal host for high-performance sodium-sulfur batteries and hydrogen storage, Energy Stor. Mater. 14 (2018) 314–323.
[13] L. Ouyang, K. Chen, J. Jiang, X.-S. Yang, M. Zhu, Hydrogen storage in light-metal based systems: a review, J. Alloys Compd. 829 (2020) 154597.
[14] Y.R. Wang, X.W. Chen, H.Y. Zhang, G.L. Xia, D.L. Sun, X.B. Yu, Heterostructures built in metal hydrides for advanced hydrogen storage reversibility, Adv. Mater. 32 (2020) 2002647.
[15] Q.F. Meng, Y.Q. Huang, J.K. Ye, G.L. Xia, G.F. Wang, L.X. Dong, Z.X. Yang, X.B. Yu, Electrospun carbon nanofibers with in-situ encapsulated Ni nanoparticles as catalyst for enhanced hydrogen storage of MgH_2, J. Alloys Compd. 851 (2021) 156874.
[16] A. Züttel, P. Wenger, S. Rentsch, P. Sudan, P. Mauron, C. Emmenegger, $LiBH_4$ a new hydrogen storage material, J. Power Sources 118 (2003) 1–7.
[17] A. Züttel, S. Rentsch, P. Fischer, P. Wenger, P. Sudan, P. Mauron, C. Emmenegger, Hydrogen storage properties of $LiBH_4$, J. Alloys Compd. 356–357 (2003) 515–520.
[18] R. Wu, X. Zhang, Y. Liu, L. Zhang, J. Hu, M. Gao, H. Pan, A unique double-layered carbon nanobowl-confined lithium borohydride for highly reversible hydrogen storage, Small 16 (2020) 2001963.
[19] K. Xian, B. Nie, Z. Li, M. Gao, Z. Li, C. Shang, Y. Liu, Z. Guo, H. Pan, TiO_2 decorated porous carbonaceous network structures offer confinement, catalysis and thermal conductivity for effective hydrogen storage of $LiBH_4$, Chem. Eng. J. 407 (2021) 127156.
[20] J.J. Vajo, S.L. Skeith, F. Mertens, Reversible storage of hydrogen in destabilized $LiBH_4$, J. Phys. Chem. B 109 (2005) 3719–3722.
[21] J. Zhu, Y. Mao, H. Wang, J. Liu, L. Ouyang, M. Zhu, Reaction route optimized $LiBH_4$ for high reversible capacity hydrogen storage by tunable surface-modified AlN, ACS Appl. Energy Mater. 3 (2020) 11964–11973.
[22] X. Zhang, L. Zhang, W. Zhang, Z. Ren, Z. Huang, J. Hu, M. Gao, H. Pan, Y. Liu, Nano-synergy enables highly reversible storage of 9.2 wt% hydrogen at mild conditions with lithium borohydride, Nano Energy 83 (2021) 105839.
[23] S. Orimo, Y. Nakamori, G. Kitahara, K. Miwa, N. Ohba, S. Towata, A. Züttel, Dehydriding and rehydriding reactions of $LiBH_4$, J. Alloys Compd. 404–406 (2005) 427–430.
[24] P. Mauron, F. Buchter, O. Friedrichs, A. Remhof, M. Bielmann, C.N. Zwicky, A. Züttel, Stability and reversibility of $LiBH_4$, J. Phys. Chem. B 112 (2008) 906–910.
[25] Y. Yan, H. Wang, M. Zhu, W. Cai, D. Rentsch, A. Remhof, Direct rehydrogenation of $LiBH_4$ from H-deficient $Li_2B_{12}H_{12-x}$, Crystals 8 (2018) 131.
[26] Z. Ding, Y. Lu, L. Li, L. Shaw, High reversible capacity hydrogen storage through Nano-$LiBH_4$ + Nano-MgH_2 system, Energy Stor. Mater. 20 (2019) 24–35.
[27] N. Bergemann, C. Pistidda, M. Uptmoor, C. Milanese, A. Santoru, T. Emmler, J. Puszkiel, M. Dornheim, T. Klassen, A new mutually destabilized reactive hydride system: $LiBH_4$–Mg_2NiH_4, J. Energy Chem. 34 (2019) 240–254.
[28] J. Zhu, H. Wang, L. Ouyang, M. Zhu, A dehydrogenation mechanism through substitution of H by D in $LiBH_4$–MgD_2 mixture, Int. J. Hydrogen Energy 42 (2017) 3130–3135.
[29] X.B. Yu, G.L. Xia, Z.P. Guo, H.K. Liu, Dehydrogenation/rehydrogenation mechanism in aluminum destabilized lithium borohydride, J. Mater. Res. 24 (2009) 2720–2727.
[30] G.L. Xia, X.B. Yu, Z. Wu, Effects of Al adding on the reversible hydrogen properties in $LiBH_4$/Al system, Xiyou Jinshu Cailiao Yu Gongcheng/Rare Metal Materials and Engineering 38 (2009) 1618–1621.
[31] Y. Zhang, Q. Tian, J. Zhang, S.-S. Liu, L.-X. Sun, The dehydrogenation reactions and kinetics of 2LiBH4–Al composite, J. Phys. Chem. C 113 (2009) 18424–18430.
[32] O. Friedrichs, J.W. Kim, A. Remhof, F. Buchter, A. Borgschulte, D. Wallacher, Y.W. Cho, M. Fichtner, K.H. Oh, A. Zuttel, The effect of Al on the hydrogen sorption mechanism of $LiBH_4$, Phys. Chem. Chem. Phys. 11 (2009) 1515–1520.
[33] Y.J. Choi, J. Lu, H.Y. Sohn, Z.Z. Fang, Reaction mechanisms in the Li_3AlH_6/$LiBH_4$ and Al/$LiBH_4$ systems for reversible hydrogen storage. Part 1: H capacity and role of Al, J. Phys. Chem. C 115 (2011) 6040–6047.
[34] M. Meggouh, D.M. Grant, G.S. Walker, Optimizing the destabilization of $LiBH_4$ for hydrogen storage and the effect of different Al sources, J. Phys. Chem. C 115 (2011) 22054–22061.
[35] D.B. Ravnsbæk, T.R. Jensen, Mechanism for reversible hydrogen storage in $LiBH_4$–Al, J. Appl. Phys. 111 (2012) 112621.
[36] Q. He, D. Zhu, X. Wu, D. Dong, X. Jiang, M. Xu, The dehydrogenation mechanism and reversibility of $LiBH_4$ doped by active Al derived from AlH_3, Metals 9 (2019).
[37] Y. Li, S. Wu, D. Zhu, J. He, X. Xiao, L. Chen, Dehydrogenation performances of different Al source composite systems of $2LiBH_4 + M$ (M = Al, $LiAlH_4$, Li_3AlH_6), Front. Chem. 8 (2020).
[38] B.R.S. Hansen, D.B. Ravnsbæk, D. Reed, D. Book, C. Gundlach, J. Skibsted, T.R. Jensen, Hydrogen storage capacity loss in a $LiBH_4$–Al composite, J. Phys. Chem. C 117 (2013) 7423–7432.
[39] A. Andreasen, T. Vegge, A.S. Pedersen, Dehydrogenation kinetics of as-received and ball-milled $LiAlH_4$, J. Solid State Chem. 178 (2005) 3672–3678.
[40] O. Friedrichs, A. Borgschulte, S. Kato, F. Buchter, R. Gremaud, A. Remhof, A. Züttel, Low-temperature synthesis of $LiBH_4$ by gas–solid reaction, Chem. Eur J. 15 (2009) 5531–5534.
[41] G.L. Xia, Y.B. Tan, X.W. Chen, F. Fang, D.L. Sun, X.G. Li, Z.P. Guo, X.B. Yu, Oxygen-free layer-by-layer assembly of lithiated composites on graphene for advanced hydrogen storage, Adv. Sci. 4 (2017) 166257.
[42] J. Xu, R. Meng, J. Cao, X. Gu, Z. Qi, W. Wang, Z. Chen, Enhanced dehydrogenation and rehydrogenation properties of $LiBH_4$ catalyzed by graphene, Int. J. Hydrogen Energy 38 (2013) 2796–2803.
[43] G.L. Xia, Y.B. Tan, F.L. Wu, F. Fang, D.L. Sun, Z.P. Guo, Z.G. Huang, X.B. Yu, Graphene-wrapped reversible reaction for advanced hydrogen storage, Nano Energy 26 (2016) 488–495.
[44] A. Gasnier, M. Luguet, A.G. Pereira, H. Troiani, G. Zampieri, F.C. Gennari, Entanglement of N-doped graphene in resorcinol-formaldehyde: effect over nanoconfined $LiBH_4$ for hydrogen storage, Carbon 147 (2019) 284–294.
[45] F. Esposto, K. Griffiths, P. Norton, R. Timsit, Simple source of Li metal for evaporators in ultrahigh vacuum (UHV) applications, J. Vac. Sci. Technol. 12 (1994) 3245–3247.
[46] G. Mavel, J. Escard, P. Costa, J. Castaing, ESCA surface study of metal borides, Surf. Sci. 35 (1973) 109–116.
[47] D.A. Hensley, S.H. Garofalini, XPS investigation of lithium borate glass and the Li/$LiBO_2$ interface, Appl. Surf. Sci. 81 (1994) 331–339.
[48] R. Gosalawit-Utke, S. Meethom, C. Pistidda, C. Milanese, D. Laipple, T. Saisopa, A. Marini, T. Klassen, M. Dornheim, Destabilization of $LiBH_4$ by nanoconfinement in PMMA–co–BM polymer matrix for reversible hydrogen storage, Int. J. Hydrogen Energy 39 (2014) 5019–5029.
[49] K. Wang, X. Kang, Q. Kang, Y. Zhong, C. Hu, P. Wang, Improved reversible dehydrogenation of $2LiBH_4$–MgH_2 composite by the controlled formation of transition metal boride, J. Mater. Chem. 2 (2014) 2146–2151.
[50] A. Gasnier, G. Amica, J. Juan, H. Troiani, F.C. Gennari, N-doped graphene-rich aerogels decorated with nickel and cobalt nanoparticles: effect on hydrogen storage properties of nanoconfined $LiBH_4$, J. Phys. Chem. C 124 (2020) 115–125.